BEHAVIOUR OF CHARACTERISITC MODES ON PATCH ANTENNAS IN MULTILAYERED MEDIA

Michael F. Adamson[1,2], Ivor L. Morrow[2] and David James[2]
[1]DSTL, Porton Down, Salisbury, Wiltshire SP4 0JQ.
[2]EWIC, Cranfield University, Bedfordshire, MK43 0TR.

Abstract

A design methodology is described supported by Characteristic Mode Analysis (CMA) to enhance the radiation gain from a patch antenna using multiple dielectric superstrates. Analytic expressions for the radiation field patterns and impedance match are derived for the patch eigenmodes. An equivalent commercial simulation model is used to determine the associated characteristic modes. Eigenmode and CMA behaviour are studied as low cost planar dielectric sheets are stacked above the antenna to affect an increase in the radiated field gain. Numerical results are compared with laboratory measurements made on several prototype dielectric radome antenna configurations and demonstrate an impedance bandwidth of 3.6% and radiated field pattern gain of 11.5dBi for a double layer superstrate antenna.

I. INTRODUCTION

Eigenmode expansion method (EEM), singularity expansion method (SEM), and characteristic mode analysis (CMA) are three common modal analysis methods in electromagnetic engineering. CMA is being used to find other kinds of modes and resonances in the real frequency domain. The CMA was initially defined by Garbacz and Turbin [1] and was refined soon after by Harrington and Mautz [2] through diagonalizing the electric field integral equation (EFIE) operator for metallic bodies. However, compared to the eigenmodes and the natural modes the characteristic values and characteristic currents of characteristic modes are both real, which facilitates their manipulation and interpretation. More importantly, the characteristic values of characteristic modes represent the ratio between the net stored power and the radiated power. Hence, the resonant behaviors can be accurately predicted by the characteristic values.

CMA has recently found applications in the design of antennas systems that exploit the resonant modes of the mounting structure to enhance radiation properties on vehicle mounted antennas [3], [4], in the co-design of an Unmanned Aerial Vehicle (UAV) to dynamically steer the radiation pattern of a structural antenna by manipulating the characteristic modes [5] and co-design of either multiple antennas or a single multi-frequency antenna into mobile phone chassis with associated circuitry and dielectric case enclosure [6], [7], [8].

This paper describes an EEM and CMA study of a 10GHz microstrip patch antenna (MSA), in which planar dielectric superstrates are introduced to enhance the radiation pattern gain. A traditional cavity mode model is used to determine the initial resonance and impedance bandwidth for a rectangular patch antenna. An analytic cascaded transmission line model extends the analysis to include multiple stacked planar superstrates. This enables the approximate location height for planar sheets and their resultant radiation patterns to be determined. A CST Microwave Studio (CST) commercial full wave model of the patch antenna and superstrates geometry is also developed to refine the analytic results and provide CMA calculated resonant frequencies, real current sheets and radiated fields for patch antenna with and without superstrates which allows optimisation of the model geometry specifically the resonant

frequency and optimum antenna radiated fields. Several prototype antenna system were manufactured and laboratory measurements made on impedance bandwidth, dielectric superstrate height and radiation patterns. Summary conclusions are made on the use of CMA as an analysis tool and future research activity proposed.

II. Analysis of Patch Antenna and Cascaded Superstrate Structure

A. TLM Model of the Microstrip Antenna

The transmission line model (TLM) for a rectangular patch antenna is well known [9] and for brevity its detail is not repeated here. A patch antenna was designed to resonant at 10 GHz with a length of 9.06mm and width of 11.86mm on 1.588mm thick Rogers substrate ($\epsilon_r = 2.3$ and $\tan\delta = 0.001$). The TLM deduced the leading edge impedance was 228Ω and a 50Ω microstrip transmission line was quarter wavelength matched to the patch edge. The calculated patch antenna edge impedance and the impedance matched network attached to the patch edge are shown plotted against frequency in Fig 1. A commercial CST electromagnetic model was built that included the quarter wavelength matching section. Results for the simulated S_{11} response are compared with those calculated in the TLM model in Fig 2. Both models predict the resonant frequency at 10 GHz and are within 1% on the -10dB impedance bandwidth.

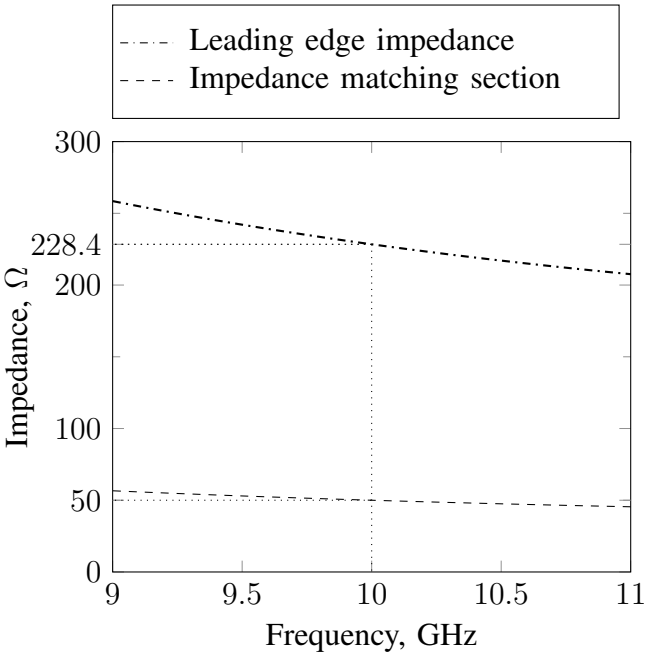

Fig. 1. Impedance versus frequency for a 10GHz resonant patch antenna at (i) the radiating edge (ii) including a $\lambda/4$ impedance matching section.

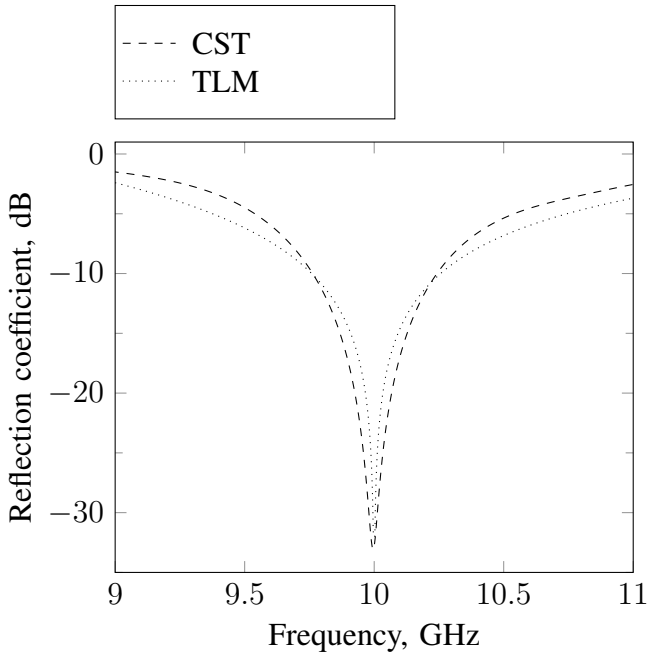

Fig. 2. Calculated S_{11} versus frequency for a 10GHz resonant patch antenna using the commercial CST model and TLM model.

B. Cavity Model of Retangular Patch Antenna

The cavity model (CM) for a rectangular patch antenna is also well known [9] and not repeated here. Using the dimensions for the patch antenna and substrate the cavity model was used to compute the modal impedance contour plots for the first few eignenmodes supported by the patch antenna. The impedance contour plots shown in Figs 3 and 4, were calculated using the cavity model [10] for the first two significant modes, TM_{01} and TM_{10}.

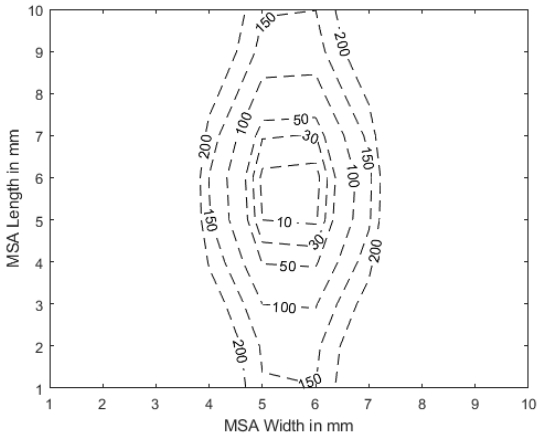

Fig. 3. Impedance contour plot for the TM_{01} mode of the patch antenna at 9.7GHz.

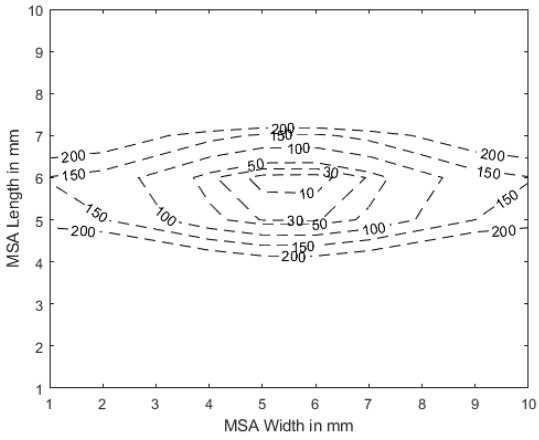

Fig. 4. Impedance contour plot for the TM_{10} mode of the patch antenna at 10GHz.

It is apparent from both modes that the impedance between the patch plates (and voltage) is a maximum at the radiating edges of the patch and a minimum at the centre of the half-wavelength long (resonant) patch antenna.

C. Characteristic Modes for Isolated Patch Antenna

CMA provide an alternative method to investigating the resonant frequencies and radiation performance of MSA where the radiation pattern is assumed to be a linear combination of the modal radiation patterns [11]. CMA are evaluated through solving the general eigenvalue equation:

$$[\vec{X}]\vec{J_n} = \lambda_n[\vec{R}]\vec{J_n} \tag{1}$$

The n$^{\text{th}}$ term eigenvectors and eigenvalues are $\vec{J_n}$ and λ_n respectively. The characteristic currents, which are the eigencurrents from which the characteristic radiation fields may be derived, are the real eigenvectors and are the source-free solution to Maxwell's equations [12], [13]. The stored field of a radiator is proportional to the magnitude of the λ_n and $\lambda_n = 0$ corresponds to a resonant mode, $\lambda_n > 0$ relates to an inductive mode, and $\lambda_n < 0$ relates to a capacitive mode where $\vec{R}$ and $\vec{X}$ are the real and imaginary parts of the antenna impedance matrix.

The CMA function (part of the CST software) was then applied to the CST model and solved at every frequency of interest to yield a full set of eigenmodes. The eigenvector generates the modal current distributions and the eigenvalues determine how capacitive or inductive the mode is and how well it radiates. The calculated eigenvalues λ_n as a function of frequency for the patch antenna are shown in Figure 5. It can readily be seen that the first mode (Mode 1) has a resonance at 9.8 GHz, a second mode has a resonance at approximately 10.25 GHz and a third mode (Mode 3) is entirely capacitive and would require additional matching to achieve resonance.

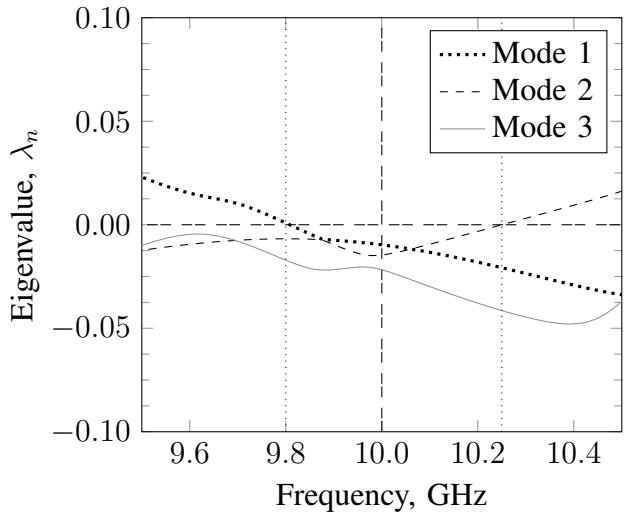

Fig. 5. Plot of the first three eigenmodes versus frequency for the isolated patch antenna.

The eigenvector modal currents for the first two modes on the patch antenna are shown in Fig 6 and Fig 7. For the TM_{10} mode both the cavity model and CMA calculations show the fields have a one to one correspondence while for the TM_{01} there is a partial maximum-to-minimum field variation across the length of the patch. The presence of the feed line affects the surface current contour plot for TM_{01} so that the current is not the same at both edges, whereas for TM_{10} the edge currents are similar.

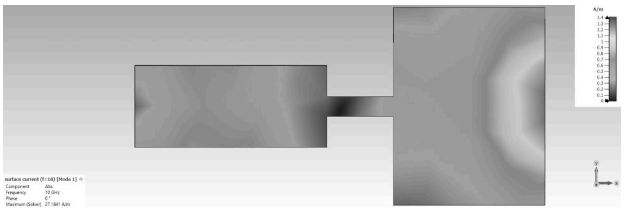

Fig. 6. Surface current contour map for the TM_{01} mode for a 10.25GHz.

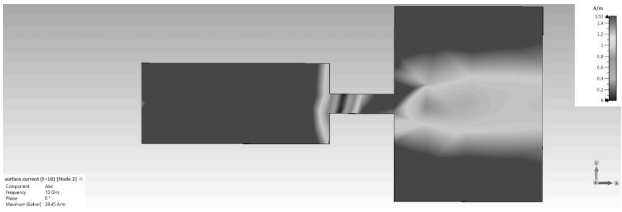

Fig. 7. Surface current contour map for the TM_{10} mode for a 9.8GHz.

D. Multilayer Superstrate Patch Antenna Analysis

It has previously been shown [14] that the introduction of planar dielectric sheet or superstrate can affect an improvement in patch antenna gain. Intuitively, the modal current on the dielectric above the patch antenna should be a maximum for a maximum radiating field. This occurs when the total electrical phase shift is, $\beta l = 2\pi/\lambda_0 \times l = \lambda_0/4$, or 90^o. If the air bridge between the patch antenna radiating surface and dielectric sheet is a height h and the dielectric sheet has a thickness B and relative dielectric constant ϵ_r then $\beta(h + B\sqrt{\epsilon_r}) = \frac{1}{4}\lambda_R$, where λ_R is the effective wavelength. To the authors knowledge, no CMA analysis of a superstrate covered patch antenna configuration as this case has been undertaken, nor has the effect of stacking more superstrates onto the structure been examined.

A polycarbonate dielectric sheet of relative dielectric constant $\epsilon_r = 3.0$ and thickness $t = 4.33$mm was introduced into the CST model and its location varied around the conditional $\frac{1}{4}\lambda_R$ height to optimize the air gap for the maximum radiated field gain. The eigenvalue problem was solved again at each frequency of interest using the CST model and Fig. 8 shows the eigenvalues for the first three modes as a function of frequency. Now, superstrate loading has evolved Mode 1 to be entirely inductive while Mode 2 and

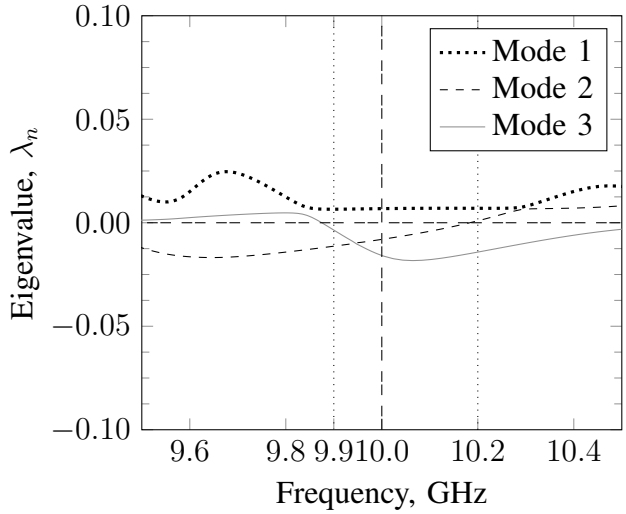

Fig. 8. CST calculated first three eigenmodes for the patch antenna with a single superstrate cover.

Mode 3 are resonant at 9.9 GHz and 10.2 GHz respectively. While the CM mode index has remained the same Mode 2 and Mode 3 correspond (i.e. have similar current distributions) to the TM_{01} and TM_{10} modes of the unloaded patch. In Fig. 9 the computed 3D radiated field pattern is plotted for the single patch antenna with superstrate at 10.0GHz, the radiation is a combination of all three modes. In Fig. 10 the 3D radiated field contribution from each individual mode at 10.0 GHz is plotted and it can readily be seen that mode 3 does not contribute significantly to the main lobe radiation.

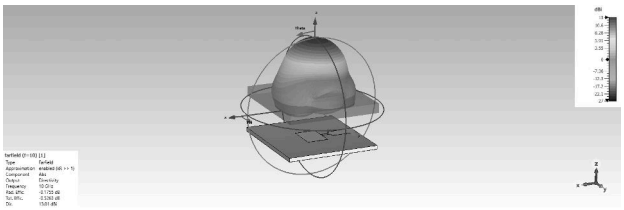

Fig. 9. CST calculated directivity for the patch antenna with a single superstrate cover.

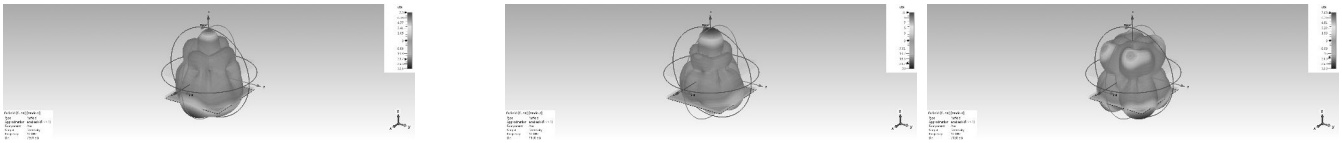

(a) Mode 1 (b) Mode 2 (c) Mode 3

Fig. 10. CST calculated radiation fields for the characteristics modes on the patch antenna with single superstrate cover.

The potential to increase the directive gain further was also investigated in a series of numerical experiments using the CST model. Additional dielectric sheets were stacked to add a second and third superstrate. The dielectric sheets were also of $\epsilon_r = 3.0$, thickness $t = 4.33$mm and located $\frac{1}{4}\lambda_R$ apart. The superstrate separations air gaps were varied again about their nominal value ($\pm$2mm) to maximise the boresight directive gain. Fig 11 demonstrates the simulated radiation patterns provide an increase in gain with each additional superstrate. However, the incremental gain decreases with successive sheets.

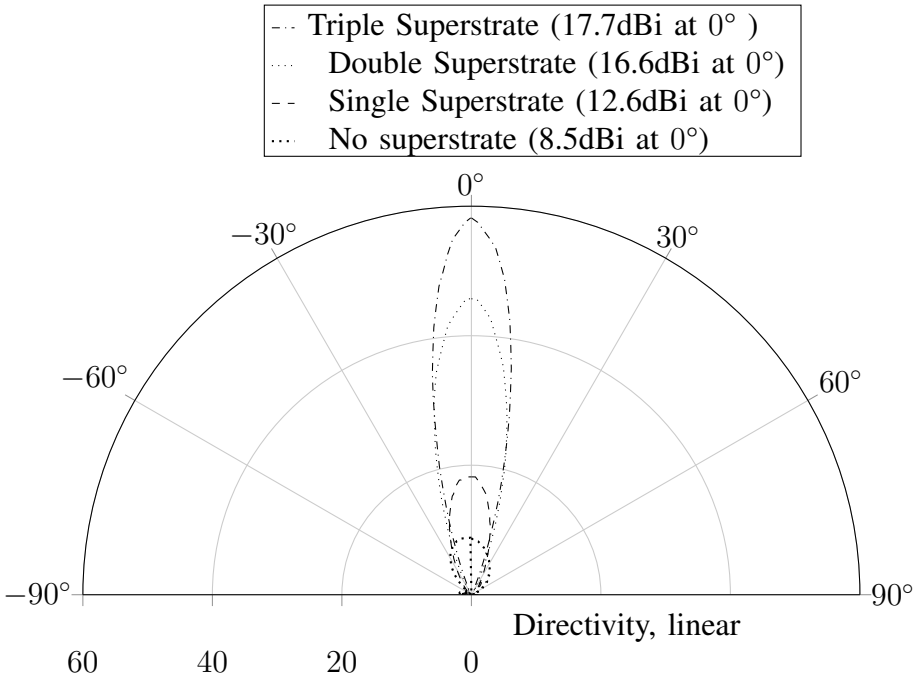

Fig. 11. CST simulated radiation pattern in the E-plane at 10 GHz for the patch antenna with (i) no superstrate, (ii) a single superstrate, (iii) a double superstrate and finally a triple superstrate radome (superstrate parameters are polycarbonate $\epsilon_r = 3.0$ and thickness $t = 4.33$mm).

III. Measured Results

A rectangular patch antenna with the dimensions calculated from the CST Model was manufactured on Rogers D-5870 substrate and is shown in Fig.12. The patch is edge fed by a printed quarter wave impedance transforming section and a 50Ω line soldered to an OSM coaxial probe connector.

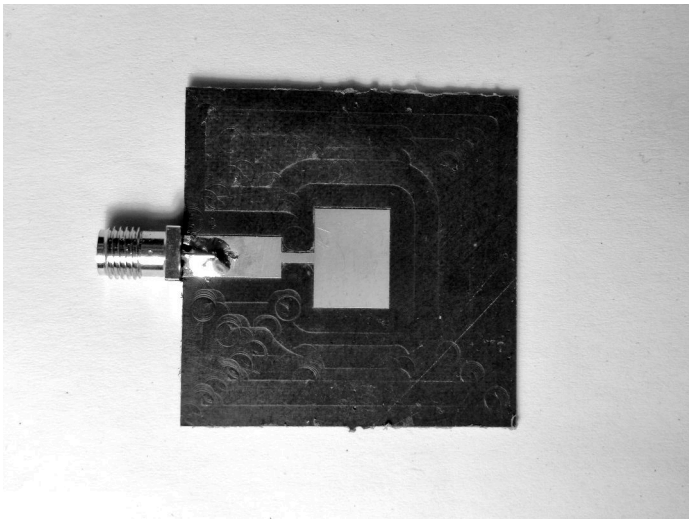

Fig. 12. The patch antenna with impedance matching section and 50Ω feed fabricated on Rogers D-5870 substrate (PCB size 4cm x 4cm).

A laboratory measurement fixture, shown in Fig 13, was setup to measure the superstrate loaded antenna impedance S_{11} and transmission S_{21} responses. The patch antenna was mounted centrally on the 40×40 centimeter aluminium ground plane. The antenna was fed via a right angled OSM coaxial connector attached to the antenna OSM launcher; this enabled the patch to be fed from below the ground plane. An

X-band Model 640 NARDA horn antenna was positioned 50cm directly above the patch and supported by polystyrene blocks as shown. Thus locating the patch and horn antenna just outside of their far-fields respectively, 12mm and 375mm. A planar polycarbonate dielectric sheet size 40×40 cm was placed above the patch antenna, and is fixed to four nylon spacers at its four corners with nylon nuts. The distance between the dielectric plate and the patch can be changed by adjusting the positions of the nylon nuts.

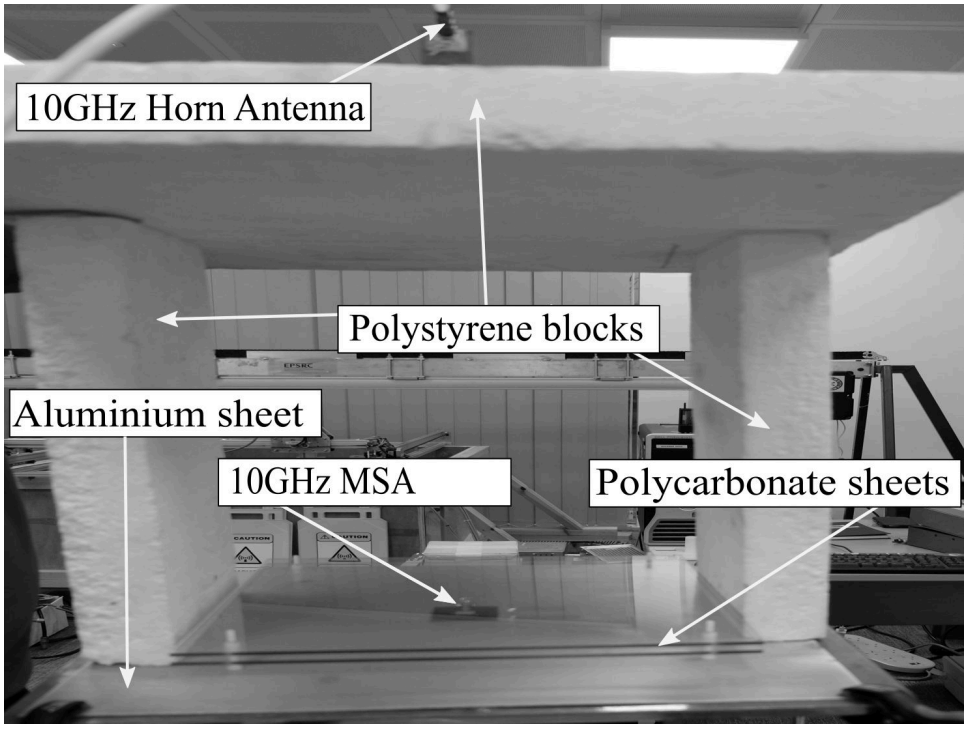

Fig. 13. Experimental Setup: The fabricated rectangular patch antenna is centrally located on a large 40×40 centimeter aluminium ground plane and probe fed from below the ground plane. Shown in the present setup are two planar polycarbonate dielectric sheets stacked at different heights above the patch antenna.

The measured S_{11} for the patch antenna, in Fig 14, shows it resonates slight higher than 9.9 GHz and around 10.13 GHz for the TM_{10} and TM_{01} modes, as compared to 9.9GHz and 10.2GHz predicted using CST . This detuning is thought to originate from reactive loading due to the coaxial connector that was not incorporated in the simulation model. The measured boresight gain as a function of frequency is shown in Fig 15 in the E plane. As can be seen from the figure the unloaded and loaded antenna resonance has shifted higher to around 10.0 GHz, thus subsequent measurement of field patterns were conducted at this frequency.

Simulations predict an incremental gain increase of around 3dB, however, experimentally we obtain a smaller 1.0dB increase per sheet as detailed in Table I. Experimentally the separation between sheets was varied by trial and error but this did not result in any further gain improvements. It is conjectured that the OSM connector (not accounted for in the simulation) is radiating and that is distorting the impressed radiated field phase fronts on the dielectric sheets.

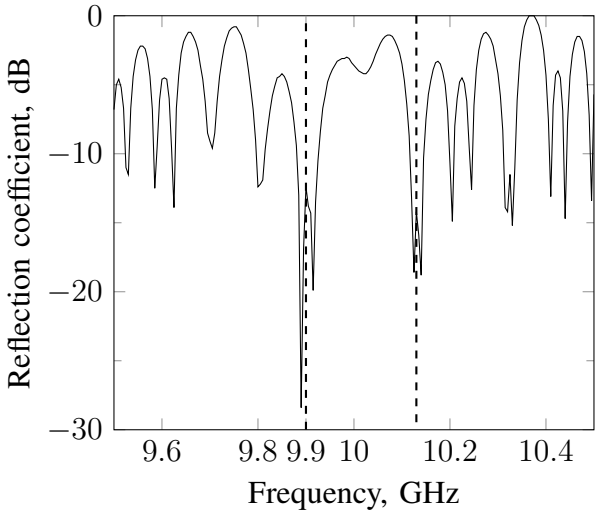

Fig. 14. Measured reflection coefficient S_{11} versus frequency for the patch antenna.

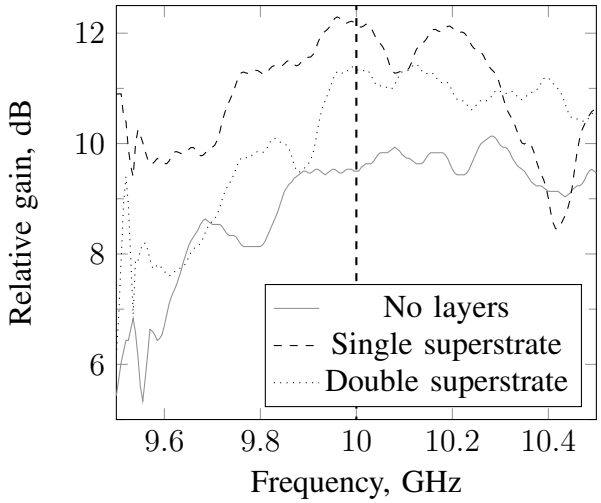

Fig. 15. Boresight gain versus frequency for the patch antenna with no or multiple superstrates.

A tapered anechoic chamber was first calibrated and then used to measure the radiated field of the patch antenna in both the E and H-plane for three different multilayer configurations that included (i) no superstrate (ii) a single planar superstrate and (iii) double planar superstrate of polycarbonate. The measured and computed directivity and (-10 dB) bandwidth results for these configurations are summarized in Table I. The measured directivity of the patch antenna is 0.7 dBi larger than predicted but both measured and simulated bandwidth increases monotonically with addition of superstrates. Table II summarises the radiation pattern characteristic as single lobed with nearly equal beamwidth in E and H-planes (not dissimilar to a horn antenna) and low sidelobe levels.

TABLE I
COMPARISON OF COMPUTED AND MEASURED DIRECTIVITY AND BANDWIDTH FOR THE MICROSTRIP PATCH ANTENNA WITH AND WITHOUT SUPERSTRATES AT 10GHZ.

Configuration	Directivity CST, dBi	Directivity E-plane Measured, dBi	BW CST, %
Double superstrate	16.6	12	3.6
Single superstrate	12.6	11	3.4
w/o superstrate	8.3	10.1	1.6

TABLE II
COMPARISON OF BEAMWIDTH, SIDELOBE LEVEL AND CROSS POLAR FIELD LEVELS FOR SINGLE, DOUBLE AND WITHOUT SUPERSTRATE PATCH ANTENNA AT 10 GHZ.

	E-plane		H-plane	
	Beamwidth	SLL, dB	Beamwidth	X-pol, dB
Double superstrate	53°	-9.5	53°	not measured
Single superstrate	65°	-9	72°	not measured
patch antenna	66°	-7.2	74°	-24.6

The polar radiation patterns for the principle planes as a function of multilayer configuration are plotted in Figs 16 and 17. As predicted the gain improves with successive superstrate layers, however, the measured gain dips on boresight in both E and H-plane for the double superstrate configuration.

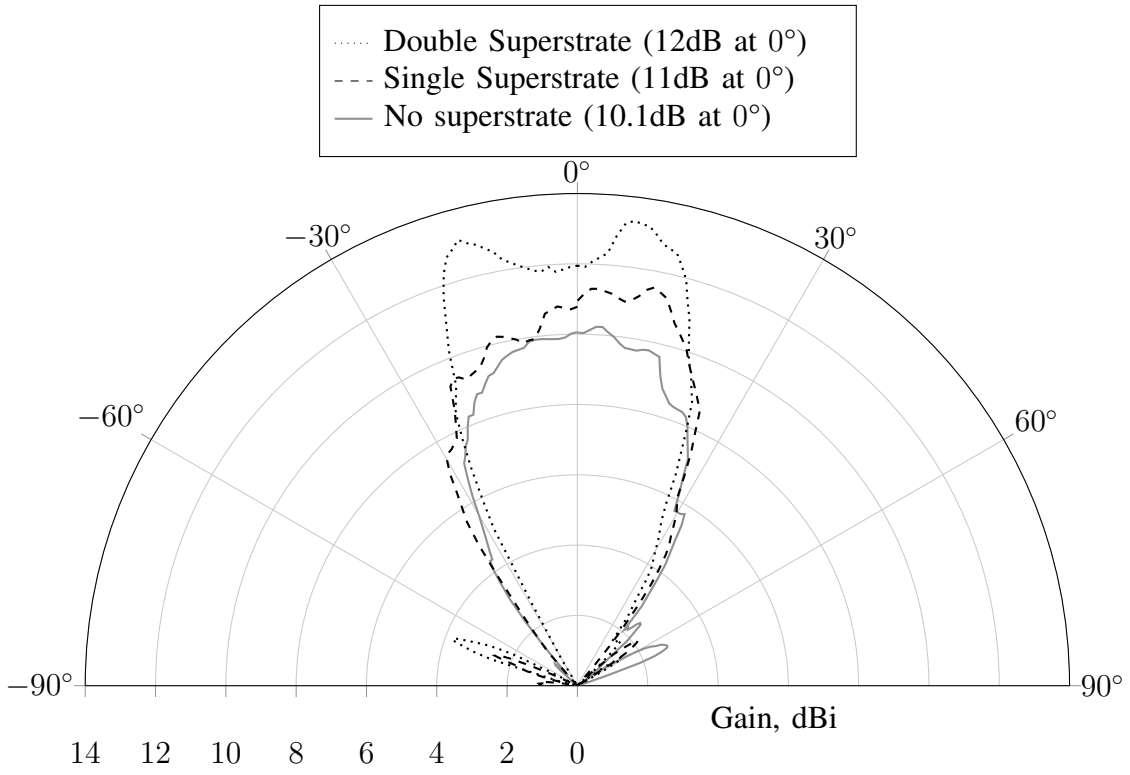

Fig. 16. E-plane radiation patterns for a patch antenna without and with single and double polycarbonate superstrates.

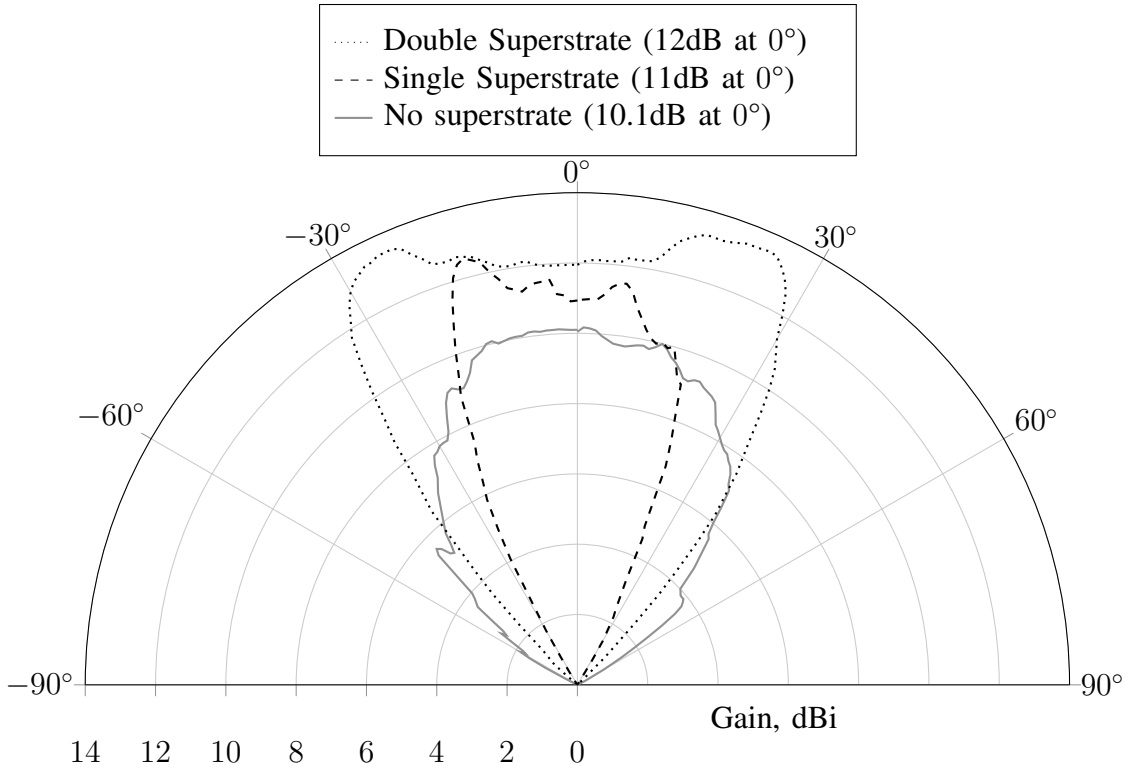

Fig. 17. H-plane radiation patterns for a patch antenna without and with single and double polycarbonate superstrates.

IV. Conclusions

The impedance bandwidth, radiation pattern, and gain for a patch antenna with multilayer superstrates has been examined. Simulation demonstrated the addition of a planar dielectric superstrate can effect up to 3.0dBi gain enhancement. Beneficial increments in gain were feasible for single, double and triple stacked superstrates but taper off with additional superstrates. Experimentally, the superstrate gain improvements obtained were smaller than predicted. Some distortion of radiation patterns was also apparent and these undesirable features are attributed to radiation from the microstrip feed perturbing the fields. The impedance bandwidth for the superstrate configurations is almost double that of the uncovered patch antenna. The inherent wider impedance bandwidth of the superstrate covered patch antenna can be an advantage to decrease the complexity of a real array.

The CMA analysis provided a unique investigation of the radiation behaviour of patch antenna with multiple dielectric radome covers and indicated the potential utility of CMA for analyzing other radiating systems. The calculated characteristic modal frequencies for the patch antenna with and without superstrate covers showed good agreement with measurements.

Acknowledgment

Michael Adamson acknowledges the support received for his studies from his employer, DSTL. The authors acknowledge the use of UK Government test facilities.

References

[1] R. Garbacz and R. Turpin, "A generalized expansion for radiated and scattered fields," *IEEE Transactions on Antennas and Propagation*, vol. 19, no. 3, pp. 348–358, 1971.

[2] R. F. Harrington and J. R. Mautz, "Computation of Characteristic Modes for Conducting Bodies," *IEEE Trans. Antennas Propag.*, vol. 19, no. 5, pp. 629–639, 1971.

[3] B. A. Austin and K. P. Murray, "The application of characteristic-mode techniques to vehicle-mounted NVIS antennas," *IEEE Antennas Propag. Mag.*, vol. 40, no. 1, pp. 7–21, 1998.

[4] T. Y. Shih and N. Behdad, "Bandwidth Enhancement of Platform-Mounted HF Antennas Using the Characteristic Mode Theory," *IEEE Trans. Antennas Propag.*, vol. 64, no. 7, pp. 2648–2659, jul 2016.

[5] S. M. Sow, L. Guo, S. G. Zhou, and T. H. Chio, "Electrically small structural antenna design for small UAV based on characteristics modes," in *2017 11th Eur. Conf. Antennas Propagation, EUCAP 2017*. Institute of Electrical and Electronics Engineers Inc., may 2017, pp. 2134–2138.

[6] N. Akiyama, N. Michishita, H. Morishita, H. Satoh, and Y. Koyanagi, "Characteristic mode analysis for small handset antenna," in *2017 Int. Symp. Antennas Propagation, ISAP 2017*, vol. 2017-Janua. Institute of Electrical and Electronics Engineers Inc., dec 2017, pp. 1–2.

[7] G. Shaker and S. Safavi-Naeini, "Antenna design for smartphones using modal/Eigenmode analysis," in *2017 11th Eur. Conf. Antennas Propagation, EUCAP 2017*. Institute of Electrical and Electronics Engineers Inc., may 2017, pp. 3457–3460.

[8] P. Liang and Q. Wu, "Characteristic Mode Analysis of Antenna Mutual Coupling in the Near Field," *IEEE Trans. Antennas Propag.*, vol. 66, no. 7, pp. 3757–3762, jul 2018.

[9] C. A. Balanis, *Advanced engineering electromagnetics*. John Wiley & Sons, 2012.

[10] K. R. Carver and J. W. Mink, "Microstrip Antenna Technology," *IEEE Trans. Antennas Propag.*, vol. 29, no. 1, pp. 2–24, 1981.

[11] R. J. Garbacz, "Modal Expansions for Resonance Scattering Phenomena," *Proc. IEEE*, vol. 53, no. 8, pp. 856–864, 1965.

[12] R. F. Harrington and J. R. Mautz, "Theory of Characteristic Modes for Conducting Bodies," *IEEE Trans. Antennas Propag.*, vol. 19, no. 5, pp. 622–628, 1971.

[13] J. Adams and J. T. Bernhard, "Eigenmode Based Circuit Models for Antennas," no. September 2012, 2012.

[14] Jackson, David R. Alexopoulos, N, "Fundamental Superstrate Effects on Printed Circuit Antennas Using Magnetic Superstrates," pp. 475–476, 1984.

Behaviour of characteristic modes on patch antennas in multilayered media

Adamson, Michael F.

2022-04-26

Adamson MF, Morrow IL, James D. (2022) Behaviour of characteristic modes on patch antennas in multilayered media. In: Automated RF (Radio Frequency) and Microwave Society (ARMMS) Conference, Thame, 25-26 April 2022

https://www.armms.org/conferences/?conference=73